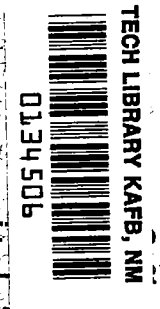

NASA Technical Paper 1137

Development and Application of an Optimization Procedure for Flutter Suppression Using the Aerodynamic Energy Concept

E. Nissim and I. Abel

FEBRUARY 1978

NASA

NASA Technical Paper 1137

Development and Application of an Optimization Procedure for Flutter Suppression Using the Aerodynamic Energy Concept

E. Nissim

Technion - Israel Institute of Technology
Haifa, Israel

and

I. Abel

Langley Research Center
Hampton, Virginia

National Aeronautics
and Space Administration

**Scientific and Technical
Information Office**

1978

SUMMARY

An optimization procedure is developed based on the responses of a system to continuous gust inputs. The procedure uses control law transfer functions which have been partially determined by using the relaxed aerodynamic energy approach. The optimization procedure yields a flutter suppression system which minimizes control surface activity in a gust environment. The procedure is applied to wing flutter of a drone aircraft to demonstrate a 44-percent increase in the basic wing flutter dynamic pressure. It is shown that a trailing-edge control system suppresses the flutter instability over a wide range of subsonic Mach numbers and flight altitudes. Results of this study confirm the effectiveness of the relaxed energy approach.

INTRODUCTION

Flutter suppression systems which use active controls are known to be sensitive to changes in flight conditions and vehicle configuration. This sensitivity implies that a control system designed for one flight condition may show considerable degradation or even be unstable at other flight conditions (ref. 1). The original aerodynamic energy concept (ref. 2) was developed to yield active control systems which are both effective in suppressing flutter and insensitive to changing flight conditions. Insensitivity to changing flight conditions was achieved in reference 2 by imposing a sufficient but not necessary condition for stability. Results of the original derivation effectively ruled out use of a single trailing-edge control in favor of a combined leading-edge trailing-edge control system. Applications of the original aerodynamic energy concept to specific problems of flutter suppression (refs. 3 to 5) and gust alleviation (ref. 5) demonstrated the effectiveness of a leading- and trailing-edge control system and also indicated the potential of a trailing-edge control system alone to control the aeroelastic response.

Recently, a relaxed aerodynamic energy concept (ref. 6) has been developed which abandons the sufficiency condition of reference 2 and yet insures the insensitivity of the control system to changing flight conditions. The results of reference 6 show that a trailing-edge control system alone may meet the requirements of both stability and insensitivity.

The purpose of this paper is to describe results of applying the relaxed aerodynamic energy concept to a specific example using a trailing-edge control system for the suppression of symmetric flutter. Since the generalized control laws in reference 6 include a number of "free parameters" (which must be determined for the dynamic characteristics of the specific system considered), a method is developed in the present paper for determining the values of these parameters. This method minimizes control surface response to atmospheric turbulence by varying the values of the free parameters. The sensitivity of the control system to changes in flight conditions is tested by introducing changes

in flight altitude and Mach number. The two transfer functions developed in reference 6 are applied in this paper to determine their relative effectiveness.

SYMBOLS

$a_T, a_{T,i}$	control law gains
b	semi-chord length
h	vertical displacement at 30 percent of wing chord, positive in down direction
h_r	vertical displacement at fuselage reference point, positive in down direction
i	$= \sqrt{-1}$
k	reduced frequency, $\omega b/V$
M	Mach number
n	number of degrees of freedom of elastic system
q	dynamic pressure
$Q(s)$	polynomial in s
s	$= i\omega$
V	flight speed
X,Y,Z	coordinate axes
α	oscillatory angle of attack of wing, positive nose up
α_r	oscillatory angle of attack at fuselage reference point, positive nose up
γ_j	aerodynamic lag terms
δ	control surface deflection, positive in down direction
ζ	damping coefficient
$\zeta_{T,i}$	free parameter associated with damping in transfer function
ρ	fluid density
ω	oscillatory frequency

$\omega_{n,T,i}$ free parameter associated with frequency in transfer function

ω_R reference frequency

Matrices:

$[A]$ complex aerodynamic matrix

$[A_j]$ real aerodynamic matrix coefficients

$[D_j]$ real aerodynamic matrix coefficients

$\{F_G\}$ aerodynamic gust force vector

$[F_j]$ real coefficients of equations of motion

$[K]$ structural stiffness matrix

$[M]$ generalized mass matrix

$\{q\},\{\bar{q}\}$ complex response vectors

$[T]$ transfer function matrix

$[U]$ matrix representing first-order equations of motion

$\{X\}$ response vector of first-order equations of motion

Subscripts:

f flutter

max maximum

rms root-mean-square value

Dots over symbols denote derivatives with respect to time.

CONTROL LAWS

The control laws used in this work were derived by using the relaxed energy method (ref. 6). The control laws are of the following general form:

$$\delta = \lfloor T \rfloor \begin{Bmatrix} h/b \\ \alpha \end{Bmatrix} \tag{1}$$

where $\lfloor T \rfloor$ is a transfer function matrix of size 1×2 and where δ, h, α, and b are defined in sketch (a). (Arrows indicate positive displacements and rotations.)

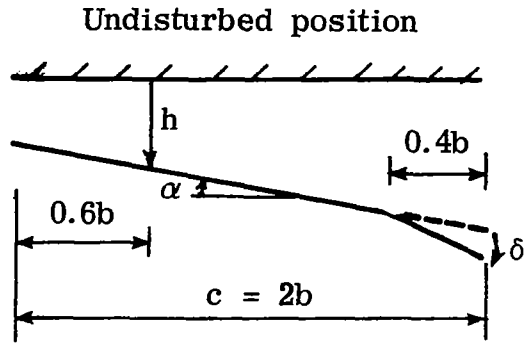

Sketch (a)

Sketch (a) represents the cross section of the center line of a streamwise strip located along the wing defined by the inboard and outboard control surface edges. The control surface has a 20 percent chord, and the wing displacement h is measured at the 30-percent chord point. Two types of transfer function matrices $\lfloor T \rfloor$ were presented in reference 6: (1) localized damping type transfer function (LDTTF), and (2) damping type transfer function (DTTF). A brief presentation of these transfer functions is made together with a description of their characteristics.

Localized Damping Type Transfer Function

The form of the localized damping type transfer function (LDTTF) is

$$\lfloor T \rfloor = \lfloor 0 \quad -1.86 \rfloor + \frac{a_T s^2}{s^2 + 2\zeta_T \omega_{n,T} s + \omega_{n,T}^2} \lfloor 4 \quad 2.8 \rfloor \qquad (2)$$

where a_T, ζ_T, and $\omega_{n,T}$ are positive free parameters. The matrix elements 0, -1.86, 4, and 2.8 were fixed by the relaxed energy method (ref. 6) for a 20-percent chord control and wing displacement measured at the 30-percent chord point. These elements can be modified to account for displacement measured at another point on the wing chord by applying a simple transformation matrix (ref. 2).

It is shown in reference 6 that a_T controls the amount of aerodynamic damping introduced by the control, $\omega_{n,T}$ determines the frequency around which the largest values of damping are introduced, and ζ_T controls the distribution of damping at frequencies around $\omega = \omega_{n,T}$. It is further shown (ref. 6) that for frequencies $\omega < \omega_{n,T}$ the LDTTF introduces into the aeroelastic system an aerodynamic inertia type term which opposes aerodynamic stiffness and for $\omega > \omega_{n,T}$ aerodynamic stiffness is added. The form of the transfer function given in equation (2) allows considerable versatility by using the free parameters to adjust the control law for a specific application.

To increase the versatility of this control concept, a modification is introduced into equation (2) which permits the damping distribution to be "peaked" at two values of frequency. This modification enables the aerodynamic stiffness to be controlled in a region of frequencies which lie between the two peaks. In addition, a wider frequency distribution of damping is available.

The resulting transfer function is

$$\lfloor T \rfloor = \lfloor 0 \quad -1.86 \rfloor + \left(\frac{a_{T,1} s^2}{s^2 + 2\zeta_{T,1}\omega_{n,T,1} s + \omega_{n,T,1}^2} + \frac{a_{T,2} s^2}{s^2 + 2\zeta_{T,2}\omega_{n,T,2} s + \omega_{n,T,2}^2} \right) \lfloor 4 \quad 2.8 \rfloor \tag{3}$$

where the subscripts 1 and 2 refer to the values of the free parameters at the first and second peak, respectively.

Damping Type Transfer Function

The form of the damping type transfer function (DTTF) is given by

$$\lfloor T \rfloor = \lfloor 0 \quad -1.86 \rfloor + \frac{a_T s}{\omega_R} \lfloor 4 \quad 3.2 \rfloor \tag{4}$$

where a_T is a single free parameter which controls the amount of damping introduced by the control surface and ω_R is a reference frequency. As in the preceding case, the matrix elements 0, -1.86, 4, and 3.2 are fixed for a 20-percent chord control and wing displacement measured at the 30 percent chord. In application made in the present work, ω_R is assigned the value of the basic wing (no control) flutter frequency. (To avoid difficulties in the numerical solution of the equations of motion, the second term in equation (4) is modified to the following form $\frac{a_T s}{\omega_R}\left(\frac{50000}{s + 50000}\right)\lfloor 4 \quad 3.2 \rfloor$. The amplitude and phase angle changes due to the introduction of this first-order filter are negligible over the range of frequencies considered in this paper.) The DTTF does not permit the introduction of aerodynamic stiffness other than the -1.86α term and, furthermore, may give rise to stability problems at high frequencies as indicated in reference 6. Nevertheless, this transfer function is applied in the present work to test its adequacy for preliminary design studies, where a small number of variables are a considerable advantage.

OPTIMIZATION PROCEDURE

Basic Concept

In the design of an active flutter suppression system, stability is not the sole objective. For example, a stable design which results in excessive control surface activity in a turbulent atmosphere may be impractical. Therefore, a more rational approach is to design a system which provides stability with minimum control surface activity (that is, minimum control surface rates or deflections). Minimum control activity is accomplished by first assigning initial values to the free parameters in either the LDTTF or DTTF transfer functions that stabilize the system above the required flutter velocity margin. (In unusual circumstances, the DTTF may be incapable of stabilizing the aeroelastic

system.) Next, the free parameters are determined by minimizing the response of the control surface to a gust input. This minimization does not result in loss of stability since experience has shown that if the free parameters are changed to reduce the stability of the system to the point where it is only marginally stable, then the control surface activity in a gust environment increases. In this manner, the gust becomes a driver in establishing the closed-loop parameters while system stability is maintained.

Target Function

A target function is defined in terms of control surface activity to allow optimization of the free parameters. Control surface activity is determined by introducing the control law into a continuous gust response analysis. The response of the control surface to atmospheric turbulence is calculated by a method similar to that described in reference 7. The target function is then defined as either the root-mean-square (rms) control deflection or the rms control surface rate per unit rms gust input based on a Von Kármán gust spectrum.

Optimization Steps

The basic steps required for optimization are

(1) Select a control law type (LDTTF or DTTF) and assign initial values to the free parameters that stabilize the aeroelastic system at the desired flight velocity and Mach number.

(2) Calculate the rms control surface activity per unit rms gust input for the control law by using a continuous gust response analysis.

(3) Determine the values of the free parameters which result in minimum control activity.

Selection of the initial values of the free parameters is not as arbitrary as it may appear. This point is discussed in subsequent sections dealing with application of the optimization procedure.

Once the type of control law is selected and the free parameters are assigned initial values which stabilize the system at a particular flight condition, the optimized control law is determined solely on the basis of a gust response analysis rather than on flutter considerations. The implications of this process are (a) reduced computational time, since there is no need to solve large eigenvalue problems associated with the flutter calculations; and (b) simplicity, since it is not necessary to follow discrete eigenvalue branches associated with each response mode.

Optimization Algorithm

The algorithm used for optimization is a variation of Stewart's adaptation of the Davidon-Fletcher-Powell method (refs. 8 and 9). The variation introduced

permits the values of the free parameters to be constrained without using penalty functions and with excellent convergence characteristics. Penalty functions are avoided by restricting the step direction in the independent variables to be tangent to a constraint boundary when (a) the boundary has been reached and (b) the unconstrained direction to a step results in constraint violation.

APPLICATION

The optimization procedure is applied to a specific example to demonstrate the procedure and to assess the effectiveness of the two transfer functions described earlier.

System Description

A flight program has been initiated by the National Aeronautics and Space Administration to study active control concepts using remotely piloted vehicles equipped with specially designed research wings (ref. 10). The optimization procedure is applied to the case of symmetrical wing flutter for this drone vehicle. A three-view drawing of the flight-vehicle—research-wing combination is shown in figure 1. Guided by results obtained during previous applications of the aerodynamic energy method (ref. 5), a control surface is placed as near to the tip of each wing as is structurally possible. Each control surface has a width of 20 percent of the local wing chord and a length of approximately 12 percent of the wing semispan.

To avoid difficulties introduced by rigid body degrees of freedom, an extended version of the control laws (ref. 5) is used in the present work. The extended version is essentially the same form as that given by equation (1) except that h/b and α are replaced by $(h - h_r)/b$ and $\alpha - \alpha_r$, respectively. These terms represent the "relative" displacement and twist of the wing with respect to a rigid fuselage. The quantities h, h_r, α, and α_r are measured at the locations indicated in figure 2.

Objectives

The following objectives were set for the active control system:

(1) The drone should be able to fly at $M = 0.9$ with a value of q_{max} which is 44 percent above the basic wing (no control) flutter dynamic pressure with minimum control activity.

(2) The stability of the system must be maintained by using fixed values for the free parameters with no substantial increase in control activity for values of $M \leq 0.9$ and $q \leq q_{max}$.

Mathematical Model

Equations of motion.- The n equations

$$\left([M]s^2 + \frac{1}{2}(\rho V^2)[A] + [K]\right)\{\bar{q}\} = \{F_G\} \tag{5}$$

represent the equations of motion. All matrices in equation (5) are of order $n \times (n + r)$ (that is, n structural modes + r controls). Two rigid-body modes and seven symmetric elastic modes are used in the present analysis. The seven elastic modes cover a frequency range of 9.9 to 128 Hz. Modes, frequencies, and generalized masses were determined from a finite-element NASTRAN model. Unsteady aerodynamic forces for the wing, horizontal tail, and control surfaces were computed for different values of Mach number and reduced frequency by using a doublet lattice aerodynamic computer program. The frequency plane aerodynamics from doublet lattice aerodynamics are then used to obtain an s plane approximation as described in the appendix. (See also ref. 11.)

Flutter solution.- Equation (5), with $\{F_G\} = 0$, can be reduced to the following series of first-order equations (see appendix for details)

$$s\{X\} = [U]\{X\} \tag{6}$$

where the matrix $[U]$ is a function of $[T]$, M, V, and dynamic pressure q. For a given Mach number, the flight velocity V varies somewhat because of the change of speed of sound with altitude. As an illustration, the speed of sound varies by about 7.6 percent in the altitude range between 0 and 6000 m. If the speed of sound is determined for a mid-range point (for example, 3000 m), variations in the speed of sound within the 0- to 6000-m range are within ±3.8 percent. Therefore, by choosing a value for M, the value of V follows (when the speed of sound is considered to be fixed at the mid-range value) and a study can be made of the variations of the eigenvalues of equation (6) with the dynamic pressure q for a given Mach number and transfer function $[T]$. The variation in q is equivalent to changes in altitude with Mach number constant. Results are presented as root locus plots where q is varied over a wide range of values.

Gust solutions.- Equation (5) allows a direct evaluation of the control activity per unit gust velocity. The power spectral density (PSD) values of control activity per unit rms gust velocity are determined by using the Von Kármán gust spectrum, with a turbulence scale of 762 m. Values (rms) of control activity are evaluated from the PSD distributions.

RESULTS AND DISCUSSION

Results for symmetric flutter of the basic wing (no controls) at various Mach numbers are presented first. These results form the basis for assessing improvements introduced by the active control system. The closed-loop results for each of the two transfer functions studied are presented and discussed separately. A comparative discussion regarding the results obtained by both transfer functions is also made.

Basic Wing Flutter

Root locus plots for $M = 0.9$, 0.7, and 0.5 are given in figures 3 to 5. Root loci for each mode are indicated in the figures. Arrows on the loci indicate increasing dynamic pressure. The value of q at flutter (q_f) is indicated in each figure. A classical flutter behavior is apparent at all three Mach numbers since the frequencies of modes 1 and 2 tend to coalesce with increasing dynamic pressure as mode 1 crosses into the unstable region at $M = 0.9$ and 0.7 and mode 2 crosses at $M = 0.5$. Flutter dynamic pressures are given in table I.

Localized Damping Type Transfer Function (LDTTF)

Initialization of free parameters.- By using equation (3), the initial values of the free parameters in the LDTTF were chosen to place one of the peaks introduced by the transfer function at a frequency above the basic wing flutter frequency and the other at a frequency below it. The flutter frequency at $M = 0.9$ is approximately 100 rad/s. The design point for the optimization study was selected to be a 44-percent increase in flutter dynamic pressure (q_{max} = 34.66 kPa) at $M = 0.9$. The following values were assigned to the free parameters in equation (3):

$$\omega_{n,T,1} = 80 \text{ rad/s}$$

$$\omega_{n,T,2} = 120 \text{ rad/s}$$

$$\zeta_{T,1} = 0.5$$

$$\zeta_{T,2} = 0.5$$

$$a_{T,1} = 1.0$$

$$a_{T,2} = 1.0$$

These initial values of a_T did not stabilize the system, and the values of a_T were increased to

$$a_{T,1} = a_{T,2} = 2.0$$

which resulted in a stable system up to q_{max}.

Optimization results.- For the first application of the optimization procedure, the free parameters were constrained within the following ranges:

$$25 \leq (\omega_{n,T,1}, \omega_{n,T,2}) \leq 200$$

$$0.25 \leq (\zeta_{T,1}, \zeta_{T,2}) \leq 1.0$$

$$0 \leq (a_{T,1}, a_{T,2}) \leq 5.0$$

At an early stage in the optimization studies, it became apparent that control surface rates were more critical from the point of view of design, and the target function was formulated in terms of minimizing control surface rates. The optimization procedure resulted in the following values of the control law:

$$\delta = \begin{bmatrix} 0 & -1.86 \end{bmatrix} + \left(\frac{3.1s^2}{s^2 + 2(0.78)(25)s + (25)^2} \right) \begin{bmatrix} 4 & 2.8 \end{bmatrix} \begin{Bmatrix} (h - h_r)/b \\ \alpha - \alpha_r \end{Bmatrix} \qquad (7)$$

In the application of equation (3), only one peak was needed to meet system requirements. This situation may not be the case in general, however, and for other applications more than one set of free parameters may be needed. By using equation (7), the minimized control surface rate and the resulting displacement at the design point were

$$\dot{\delta} = \frac{229^\circ/s}{m/s}$$

$$\delta = \frac{4.66^\circ}{m/s}$$

The form of equation (7) indicates that minimum control rates are obtained by a single "peak" (that is, $a_{T,2} = 0$) at a relatively low frequency ($\omega = 25$ rad/s). This low frequency results in significant aerodynamic stiffness being added around the basic wing flutter frequency.

Stability calculations using the control law defined by equation (7) showed that the system exhibited the required margin in dynamic pressure; however, once the control surface activity was evaluated over a range of dynamic pressures at both $M = 0.9$ and $M = 0.7$, it was apparent that the maximum control surface activity did not occur at the design point ($q_{max} = 34.66$ kPa). The variation of rms control surface activity is given in figure 6. Control surface rates increase as both Mach number and dynamic pressure are reduced. The peak value of control surface rate is around $370^\circ/s/m/s$ at $M = 0.7$ and $q = 22.8$ kPa. This deterioration is a consequence of attempting to stabilize the system with too much reliance on aerodynamic stiffness. When Mach number or flight density ρ are reduced, the aerodynamic forces which induce aerodynamic stiffness are also reduced and this reduction results in an increase of control surface activity.

This adverse control activity can be interpreted in terms of the relaxed energy approach. It is shown in reference 6 that with respect to flutter stability, the active control system is insensitive to changing flight conditions if, over a range of reduced frequency k, the following conditions are maintained:

$$\left.\begin{aligned} |\bar{\lambda}_{min}| &= \text{Near maximum value} \\ \bar{\lambda}_{max} &>> |\bar{\lambda}_{min}| \end{aligned}\right\} \tag{8}$$

where $\bar{\lambda}_{min}$ and $\bar{\lambda}_{max}$ are the smallest and the largest aerodynamic eigenvalues, respectively, derived from the two-dimensional model adopted in reference 6. Figure 7 shows a typical variation of $\bar{\lambda}_{min}$ and $\bar{\lambda}_{max}$ as a function of $1/k$ and various values of ζ_T (from ref. 6) for $M = 0.9$ with $k_{n,T} = 0.2$ (where $k_{n,T} = \omega_{n,T}b/V$).

The relaxed energy conditions for insensitivity (eq. (8)) are satisfied around the region of the $\bar{\lambda}_{max}$ peak which occurs at $1/k = 1/k_{n,T} = 5$. An inspection of equation (7) shows that when the optimized value of $\omega_{n,T}$ ($1/k_{n,T} \approx 35$) is much smaller than the basic wing flutter frequency ($1/k_f \approx 10$), the relaxed energy requirements (eq. (8)) are not satisfied in the critical flutter region of the basic wing. This situation may result in a decrease in stability at off-design points which leads to increased control surface activity. To avoid this situation, $\omega_{n,T,i}$ should be constrained to be nearer the basic wing flutter frequency. It is seen in figure 7 that the range of frequencies over which equation (8) is satisfied is dependent on the value of ζ_T. If ζ_T is constrained to be ≥ 0.5 and if $\bar{\lambda}_{max}$ is not permitted below half its peak value, for a given ζ_T, the following new approximate constraints on $\omega_{n,T}$ can be obtained:

$$0.65\omega_f \leq \omega_{n,T,i} \leq 1.45\omega_f \tag{9}$$

where ω_f is the basic wing flutter frequency. Obviously, there is some arbitrariness in setting up these constraints and they may be varied if necessary. However, they do indicate that $\omega_{n,T,i}$ must be constrained if it is desired to reduce sensitivity to changing flight conditions.

In lieu of the somewhat arbitrary nature of the constraint on $\omega_{n,T,i}$ the system was reoptimized at the design point ($M = 0.9$; $q_{max} = 34.66$ kPa) for the following ranges:

(1) $70 \leq \omega_{n,T,i} \leq 150$

(2) $60 \leq \omega_{n,T,i} \leq 150$

(3) $50 \leq \omega_{n,T,i} \leq 150$

During these optimizations, the remaining free parameters were constrained as follows:

$$0.5 \leq \zeta_{T,i} \leq 1.0$$

$$0 \leq a_{T,i} \leq 5.0$$

The results of these calculations along with the range $25 \leq \omega_{n,T,i} \leq 200$ are given in table I in terms of closed-loop flutter dynamic pressures and maximum control surface rates and displacements. (Control surface rates and dis-

placements given in table I are maximum values at a given Mach number and may not occur at the same dynamic pressure as the design point.) As indicated in table I, the maximum control activity (which occurs at $M = 0.7$ for $\omega_{n,T} = 25$) is substantially reduced by roughly the same amount for each of the reoptimized results. For illustrative purposes, the results for $60 \leqq \omega_{n,T,i} \leqq 150$ are discussed.

When the system was reoptimized at the design point $M = 0.9$ and $q_{max} = 34.66$ kPa, the following results were obtained:

$$\delta = \begin{bmatrix} 0 & -1.86 \end{bmatrix} + \left(\frac{5.0s^2}{s^2 + 2(0.95)60s + (60)^2} \right) \begin{bmatrix} 4 & 2.8 \end{bmatrix} \begin{Bmatrix} (h - h_r)/b \\ \alpha - \alpha_r \end{Bmatrix} \tag{10}$$

Control surface rates and displacements at the design point were

$$\dot{\delta} = \frac{253.2^\circ/s}{m/s}$$

$$\delta = \frac{3.8^\circ}{m/s}$$

The PSD of control surface rates and displacements are given in figure 8. The control law defined by equation (10) was introduced into the flutter calculations and checked at Mach numbers of 0.9, 0.7, and 0.5. Closed-loop root locus plots are given in figures 9 to 11. At $M = 0.9$, the closed-loop value of q_f is 42.49 kPa. The value of q_f increases as the Mach number is reduced; $q_f = 50.03$ kPa at $M = 0.7$, and $q_f = 58.41$ kPa at $M = 0.5$. At all three Mach numbers, the quantity q_f is well above the design point dynamic pressure of 34.66 kPa.

The variation of rms control activity with dynamic pressure q (for $q \leqq q_{max}$) at $M = 0.9$, 0.7, and 0.5 is given in figure 12. Control surface rates and deflections are maximum at the design point and decrease with q at all Mach numbers. A comparison of these results with figure 6 and table I indicates that even though the closed-loop flutter dynamic pressure for $\omega_{n,T} = 25$ rps is greater than that for $\omega_{n,T} = 60$ rps, the maximum control surface rates and displacements have been significantly reduced.

Damping Type Transfer Function (DTTF)

The DTTF contains only one free parameter a_T which controls the amount of damping introduced by the control system. This free parameter does not allow damping forces to be placed within a specified range of frequencies or the addition of aerodynamic stiffness terms. Application is made to test the adequacy of this transfer function for preliminary type investigations, where a small number of variables are of considerable advantage.

Initialization of free parameters.- At $M = 0.9$ and $q_{max} = 34.66$ kPa, the value of a_T was set equal to 2 and the value of ω_R was set to 100, which

is the approximate basic wing flutter frequency. For the optimization, the gain a_T was constrained within the following range:

$$0 \leq a_T \leq 5$$

Optimization results.- The results obtained for the control system at $M = 0.9$ and $q_{max} = 34.66$ kPa are

$$\dot{\delta} = \frac{241.1^\circ/s}{m/s}$$

$$\delta = \frac{3.8^\circ}{m/s}$$

The control law is

$$\delta = \begin{bmatrix} 0 & -1.86 \end{bmatrix} + \left(\frac{5s}{100}\right) \begin{bmatrix} 4 & 3.2 \end{bmatrix} \begin{Bmatrix} (h - h_r)/b \\ \alpha - \alpha_r \end{Bmatrix} \tag{11}$$

The power spectral densities of both control surface rates and displacements are given in figure 13. These distributions are similar to those obtained by using the LDTTF.

The control law defined by equation (11) was introduced into the flutter calculations and checked at Mach numbers of 0.9, 0.7, and 0.5. Closed-loop root locus plots are given in figures 14 to 16. At $M = 0.9$, the closed-loop value of $q_f = 43.67$ kPa. The value of q_f increases as the Mach number is reduced and yields $q_f = 51.23$ kPa at $M = 0.7$ and no flutter at $M = 0.5$ up to $q = 59.85$ kPa. At all Mach numbers, q_f is well above the design point dynamic pressure of 34.66 kPa.

The variation of rms control activity with dynamic pressure q (for $q \leq q_{max}$) at $M = 0.9$, 0.7, and 0.5 is given in figure 17. Control surface rates and displacements decrease with q at all Mach numbers in much the same manner as the LDTTF case.

Comparison of Results

The optimization procedure operated in a satisfactory manner for all control systems considered in this work. For all control systems, the value of dynamic pressure at flutter (q_f) was much larger than the design value q_{max}. Furthermore, no flutter instabilities developed with either changes in Mach number or dynamic pressure and no signs of instability were observed in the higher modes. To provide a comparative assessment of the various control systems, the numerical results are listed in table I. Since all control systems provided the required increase in flutter dynamic pressure, the effectiveness of each control system is judged on the basis of minimum control surface activity over a wide range of dynamic pressure and Mach number. It can be seen from table I that for those systems which use the LDTTF, the most effective are those that constrain $\omega_{n,T}$ within the limits expressed by equation (9). Even though all three of

these systems are satisfactory, it appears that the system which constrains $\omega_{n,T}$ to $60 \leq \omega_{n,T} \leq 150$ is slightly better over the dynamic pressure and Mach number range studied. The control system which used the DTTF is shown to be the most effective for this application. (The DTTF may, however, present some stability problems for other applications at very high frequencies as described in ref. 6.)

The results presented in table I show that the LDTTF with $\omega_{n,T} = 25$ resulted in the largest closed-loop flutter dynamic pressures. However, since the design objective is to fly to q_{max} with minimum control activity, the value of q_f has no value in itself as a measure of overall system performance. From the standpoint of maximum control activity, the LDTTF with $\omega_{n,T} = 25$ is the least acceptable system (at $M = 0.7$, $\delta = 4.46°/m/s$, $\dot{\delta} = 372.6°/s/m/s$). These results indicate that minimizing control activity in lieu of maximizing q_f is a rational approach to control system design.

Finally, the complete optimization process for the LDTTF with six free parameters used about the same amount of computer time as a flutter calculation at a single Mach number since it is not necessary to solve large eigenvalue problems. This fact leads to a substantial reduction in computation time for the control synthesis since there is no need to determine the flutter speed as a function of feedback control law.

SUGGESTED DESIGN PROCEDURE

The following design procedure is suggested for determining the free parameters associated with the LDTTF and DTTF.

(1) Once the initial values of the free parameters are determined, minimize the control activity by optimizing the free parmeters to the highest value of q and the highest subsonic Mach number.

(2) Constrain $\omega_{n,T,i}$ to lie between $0.65\omega_f \leq \omega_{n,T,i} \leq 1.45\omega_f$; $0.5 \leq \zeta_{T,i} \leq 1$.

(3) Determine the control surface activity over a range of flight conditions. If considerable increase in control activity is observed, repeat step (1) with a narrowed range for $\omega_{n,T,i}$. If no increase is observed, a widening of the $\omega_{n,T,i}$ range may be attempted.

(4) Check system stability over a range of flight conditions.

The design procedure using the DTTF consists of steps (1) and (4) only.

CONCLUSIONS

An optimization procedure has been developed which uses control surface response to a continuous gust in the synthesis of control laws for active flutter suppression. The procedure has been applied to the case of symmetric wing

flutter of a drone aircraft. Some important conclusions of this study are as follows:

1. The minimization of control surface response to continuous gust inputs as a driver in control law synthesis is found to be effective.

2. A design procedure has been formulated which permits control surface activity to be minimized over a wide range of flight conditions.

3. The application to symmetric flutter of a drone aircraft yields control laws that suppress flutter over a wide range of altitude and Mach number by using a trailing-edge control.

4. The results confirm the effectiveness of the relaxed aerodynamic energy method.

Langley Research Center
National Aeronautics and Space Administration
Hampton, VA 23665
January 5, 1978

APPENDIX

FORMULATION OF EQUATIONS OF MOTION FOR FLUTTER ANALYSIS WITH ACTIVE CONTROLS

Let the n equations

$$\left([M]s^2 + \frac{1}{2}\rho V^2[A] + [K]\right)\{\bar{q}\} = 0 \tag{A1}$$

represent the equations of motion of n structural modes with r activated controls where $[M]$ represents the mass matrix; $[A]$, the complex aerodynamic matrix; $[K]$, the stiffness matrix; ρ, the density of the surrounding fluid; V, the velocity of the fluid; and $\{\bar{q}\}$, the response vector. All the matrices in equation (A1) are of size $n \times (n + r)$, that is, n structural modes + r active controls. The response vector $\{\bar{q}\}$ can be expressed in terms of n structural responses and r control deflections, that is,

$$\{\bar{q}\} = \begin{Bmatrix} q \\ q_c \end{Bmatrix} \tag{A2}$$

Equation (A1) can therefore be written as

$$\left(\left[M_s \;\vdots\; M_c\right]s^2 + \frac{1}{2}\rho V^2\left[A_s \;\vdots\; A_c\right] + \left[K_s \;\vdots\; K_c\right]\right)\begin{Bmatrix} q \\ q_c \end{Bmatrix} = 0 \tag{A3}$$

where subscript s denotes a structural quantity and c, a control quantity. Assume now a control law of the form

$$\{q_c\} = [T]\{q\} \tag{A4}$$

where $[T]$ is a $r \times n$ matrix representing the transfer functions of the control law. Substitution of equation (A4) into equation (A3) yields

$$\left\{\left([M_s] + [M_c][T]\right)s^2 + \frac{\rho V^2}{2}\left([A_s] + [A_c][T]\right) + \left([k_s] + [k_c][T]\right)\right\}\{q\} = 0 \tag{A5}$$

Typically, the elements of the aerodynamic matrices A_s and A_c are available as functions of the reduced frequency k and the Mach number M whereas the transfer function matrix is a function of s, normally expressed in terms of rational polynomials in s. Let the matrix $[T]$ be expressed by

$$[T] = \frac{1}{Q(s)}[T_N] \tag{A6}$$

where Q(s) is a scalar polynomial representing the common denominator of all the T_{ij} terms and where $[T_N]$ is a matrix involving the resulting numerators (as a function of s).

APPENDIX

The variation with s of the aerodynamic matrix $\left[A_s \;\vdots\; A_c\right]$ can be approximated by the following representation:

$$[A] = [A_0] + [A_1]\left(\frac{b}{V}\right)s + [A_2]\left(\frac{b}{V}\right)^2 s^2 + \sum_{j=1}^{4} \frac{[D_j]s}{s + \frac{V}{b}\gamma_j} \tag{A7}$$

where all the matrix coefficients and the γ_j values are constants. (See ref. 11.) Substitution of equations (A6) and (A7) into equation (A5) and multiplication of the resulting equation by $Q(s)$ yields a matrix polynomial expression with s of form

$$\left([F_0] + [F_1]s + [F_2]s^2 + \ldots + [F_m]s^m\right)\{q\} = 0 \tag{A8}$$

where the matrix coefficients $[F_j]$ are functions of M, V, and dynamic pressure q. Equation (A8) can be reduced to the following canonical form for eigenvalue solution

$$s\{X\} = [U]\{X\} \tag{A9}$$

where $[U]$ is of size $(m \times n) \times (m \times n)$ defined by

$$[U] = \begin{bmatrix} \left[-F_m^{-1}F_{m-1}\right] & \left[-F_m^{-1}F_{m-2}\right] & \ldots & \left[-F_m^{-1}F_1\right] & \left[-F_m^{-1}F_0\right] \\ [I] & 0 & \ldots & 0 & 0 \\ 0 & [I] & \ldots & 0 & 0 \\ 0 & 0 & \ldots & [I] & 0 \end{bmatrix} \tag{A10}$$

and $\{X\}$ is given by

$$\{X\} = \begin{Bmatrix} s^{m-1}\{q\} \\ s^{m-2}\{q\} \\ \vdots \\ s\{q\} \\ s^0\{q\} \end{Bmatrix} \tag{A11}$$

REFERENCES

1. Wykes, John H.; and Mori, Alva S.: Techniques and Results of an Analytical Investigation Into Controlling the Structural Modes of Flexible Aircraft. AIAA Symposium on Structural Dynamics and Aeroelasticity, Aug.-Sept. 1965, pp. 419-433.

2. Nissim, E.: Flutter Suppression Using Active Controls Based on the Concept of Aerodynamic Energy. NASA TN D-6199, 1971.

3. Sandford, Maynard C.; Abel, Irving; and Gray, David L.: Development and Demonstration of a Flutter-Suppression System Using Active Controls. NASA TR R-450, 1975.

4. Nissim, E.: Flutter Suppression and Gust Alleviation Using Active Controls. TAE Rep. No. 198, Technion - Israel Inst. Technol., 1974. (Available as NASA CR-138658.)

5. Nissim, E.; Caspi, A.; and Lottati, I.: Application of the Aerodynamic Energy Concept to Flutter Suppression and Gust Alleviation by Use of Active Controls. NASA TN D-8212, 1976.

6. Nissim, E.: Recent Advances in Aerodynamic Energy Concept for Flutter Suppression and Gust Alleviation Using Active Controls. NASA TN D-8519, 1977.

7. Pratt, Kermit G.: Response of Flexible Airplanes to Atmospheric Turbulence. Performance and Dynamics of Aerospace Vehicles, NASA SP-258, 1971, pp. 439-503.

8. Stewart, G. W., III: A Modification of Davidon's Minimization Method To Accept Difference Approximations of Derivatives. J. Assoc. Comput. Mach., vol. 14, no. 1, Jan. 1967, pp. 72-82.

9. Fletcher, R.; and Powell, M. J. D.: A Rapidly Convergent Descent Method for Minimization. Comput. J., vol. 6, no. 2, July 1963, pp. 163-168.

10. Abel, Irving; Perry, Boyd, III; and Murrow, Harold N.: Synthesis of Active Controls for Flutter Suppression on a Flight Research Wing. AIAA Paper 77-1062, Aug. 1977.

11. Sevart, Francis D.: Development of Active Flutter Suppression Wind Tunnel Testing Technology. AFFDL-TR-74-126, U.S. Air Force, Jan. 1975.

TABLE I.- SUMMARY OF NUMERICAL RESULTS

Mach number	Basic wing	LDTTF				DTTF
		$70 \leq \omega_{n,T} \leq 150$ $0.5 \leq \zeta_T \leq 1$	$60 \leq \omega_{n,T} \leq 150$ $0.5 \leq \zeta_T \leq 1$	$50 \leq \omega_{n,T} \leq 150$ $0.5 \leq \zeta_T \leq 1$	$25 \leq \omega_{n,T} \leq 200$ $0.25 \leq \zeta_T \leq 1$	$0 \leq a_T \leq 5$
		$a_{T,1} = 5.0$; $a_{T,2} = 0$ $\omega_{n,T,1} = 70$; $\zeta_{T,1} = 0.92$	$a_{T,1} = 5.0$; $a_{T,2} = 0$ $\omega_{n,T,1} = 60$; $\zeta_{T,1} = 0.95$	$a_{T,1} = 5.63$; $a_{T,2} = 0$ $\omega_{n,T,1} = 50$; $\zeta_{T,1} = 0.75$	$a_{T,1} \approx 3.1$; $a_{T,2} = 0$ $\omega_{n,T,1} \approx 25$; $\zeta_{T,1} \approx 0.78$	$a_T = 5$
Flutter q, kPa						
0.9	24.07	41.66	42.49	43.33	45.49	43.67
.7	27.77	49.32	50.03	51.23	53.87	51.23
.5	29.69	57.93	58.41	59.13	>59.85	>59.85
Maximum $\dot{\delta}_{rms}$; deg/s/m/s						
0.9		261.7	253.2	245.0	255.5	241.1
.7		253.9	250.6	266.3	372.6	239.1
*.5		187.6	200.1	201.4	-----	183.4
Maximum δ_{rms}; deg/m/s						
0.9		3.74	3.80	3.77	4.66	3.80
.7		3.05	3.15	3.21	4.46	3.12
*.5		1.84	1.97	2.03	----	1.87

*q limited up to sea-level values (17.69 kPa).

Wing

Area, m^2	2.787
Airfoil	Supercritical
Thickness/Chord ratio:	
At root	0.11
At tip	0.07
Aspect ratio	6.8
Mean aerodynamic chord, m	0.688

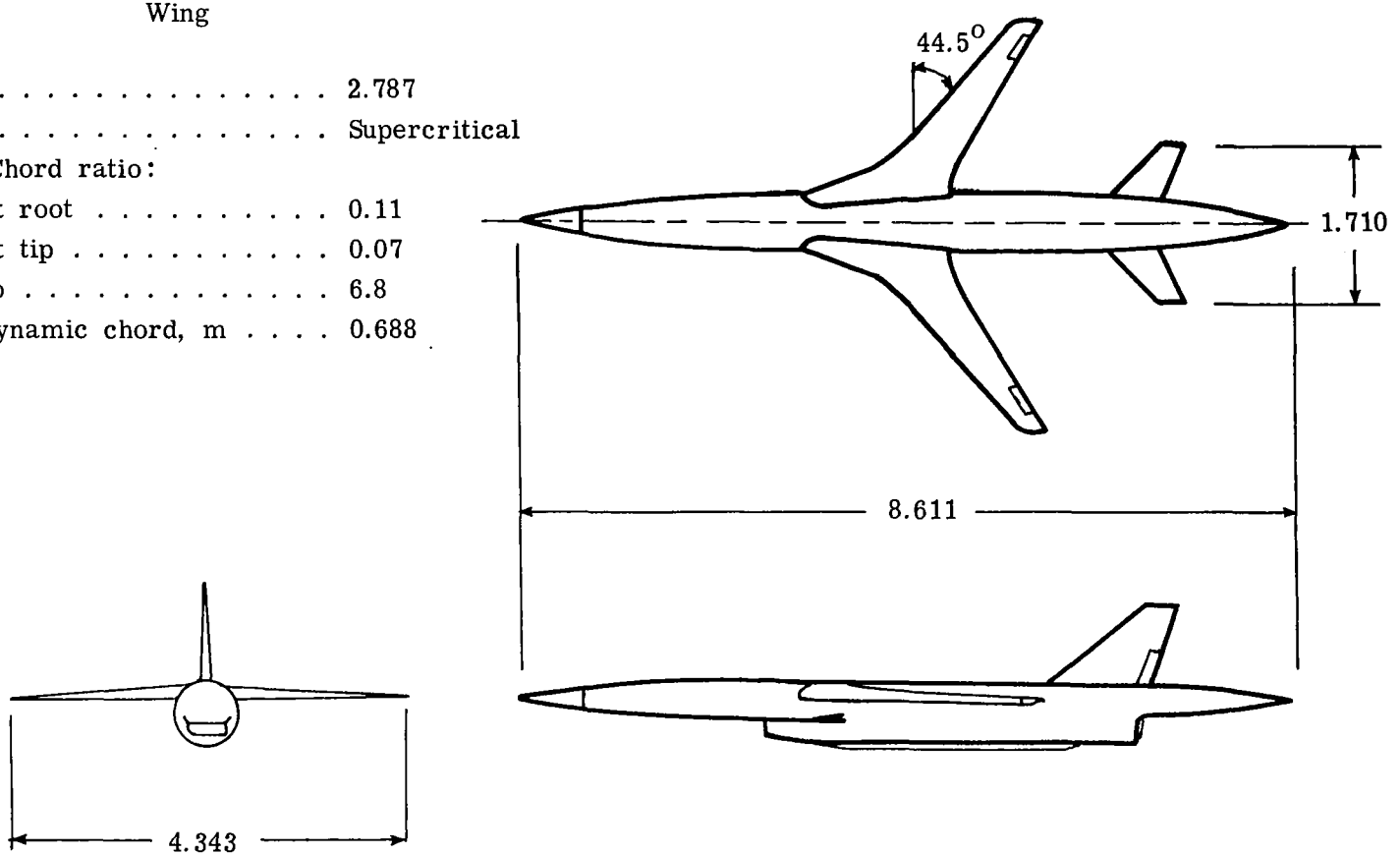

Figure 1.- Three-view drawing of drone research vehicle. All linear dimensions are in meters.

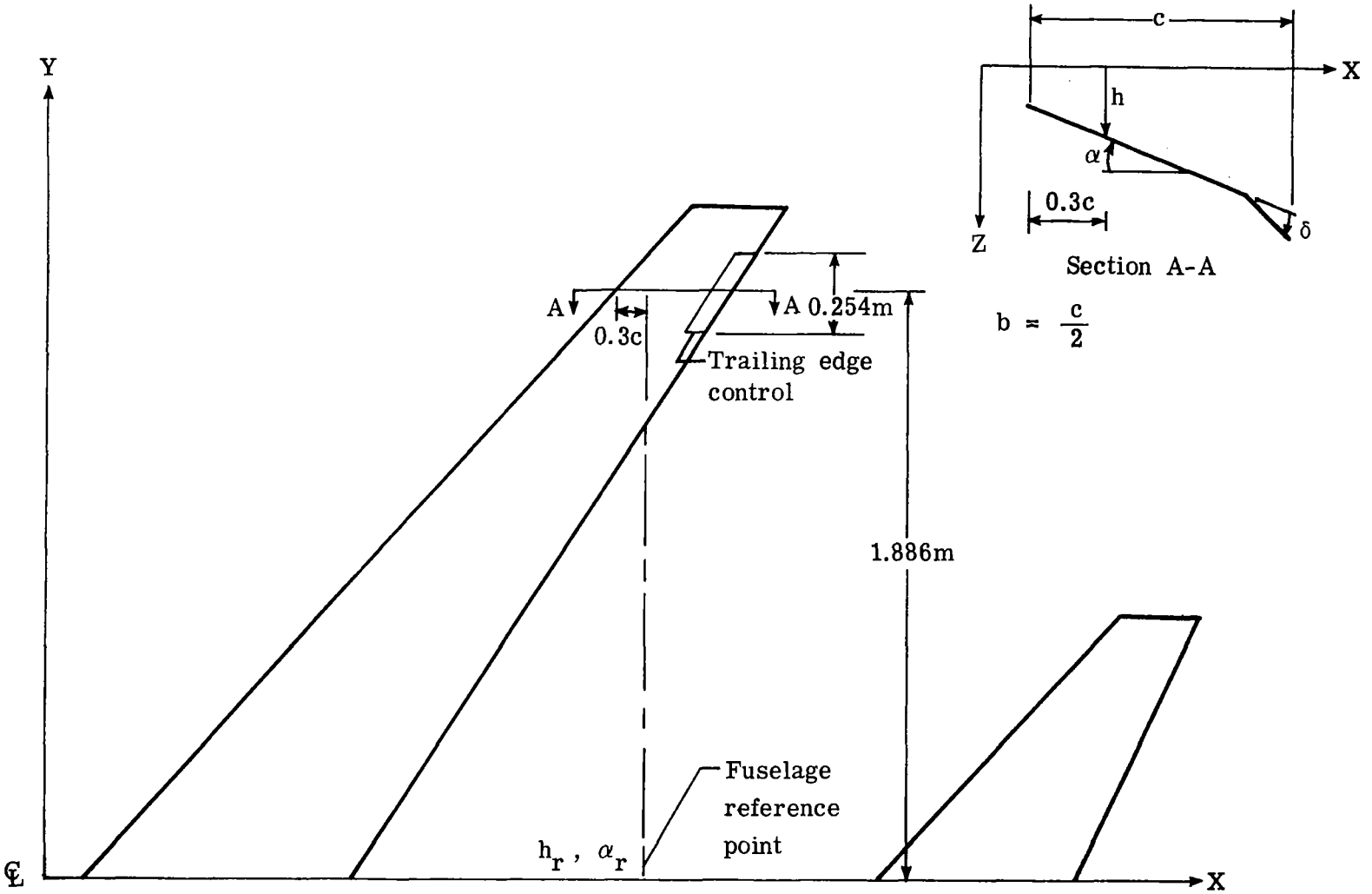

Figure 2.- Geometrical description of active control system.

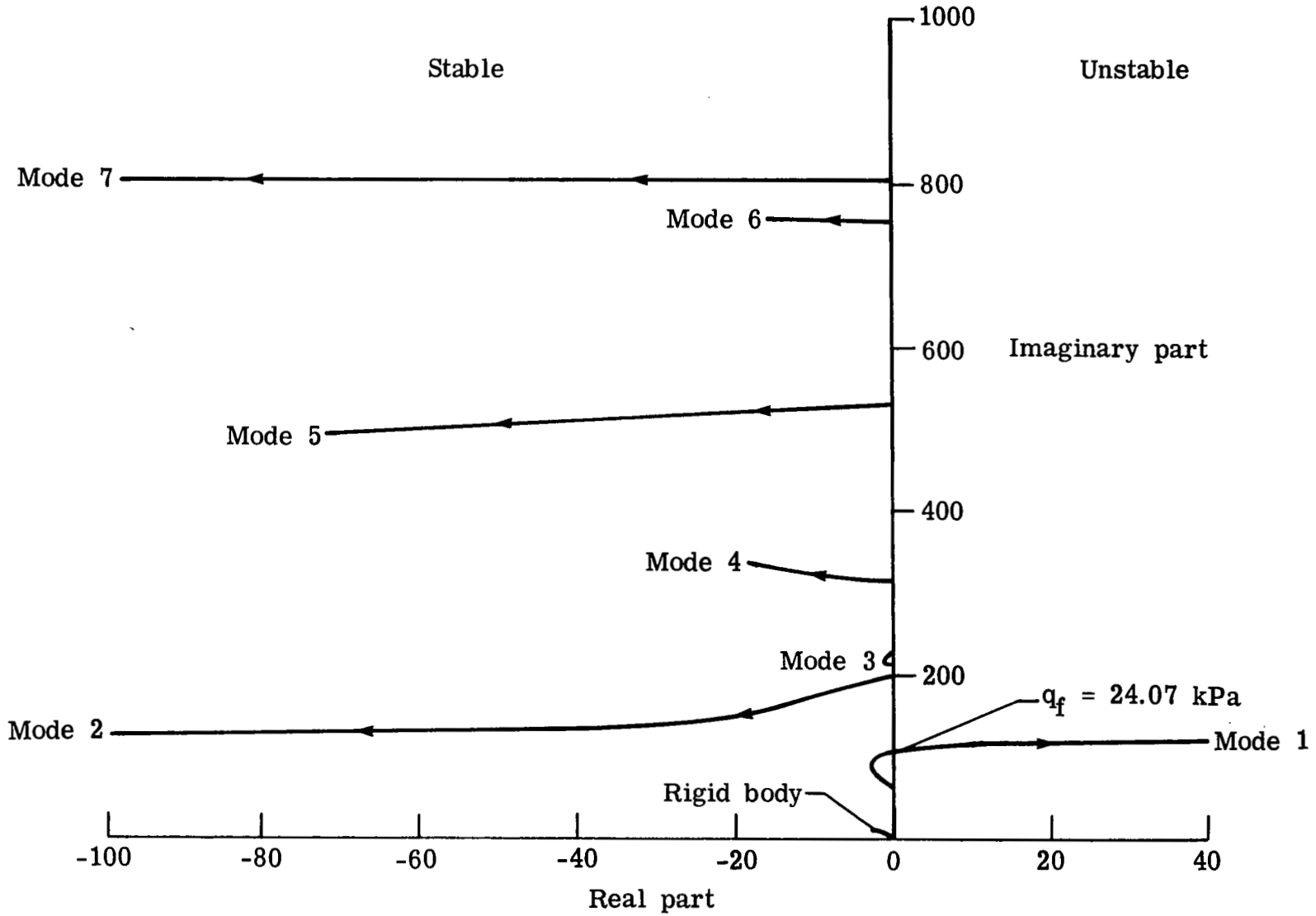

Figure 3.- Root locus plot at M = 0.9. No control. Arrows indicate increasing dynamic pressure.

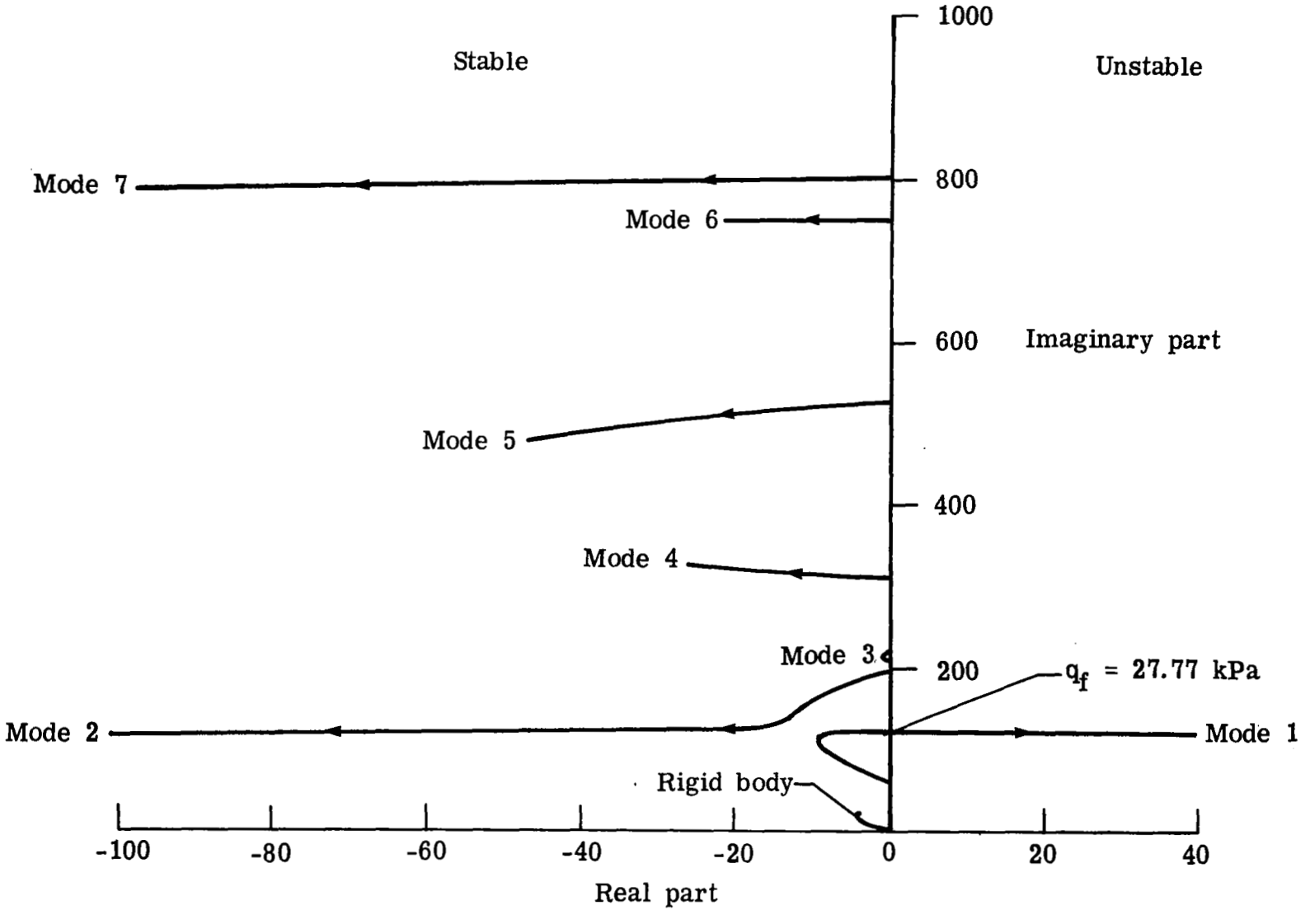

Figure 4.- Root locus plot at M = 0.7. No control. Arrows indicate increasing dynamic pressure.

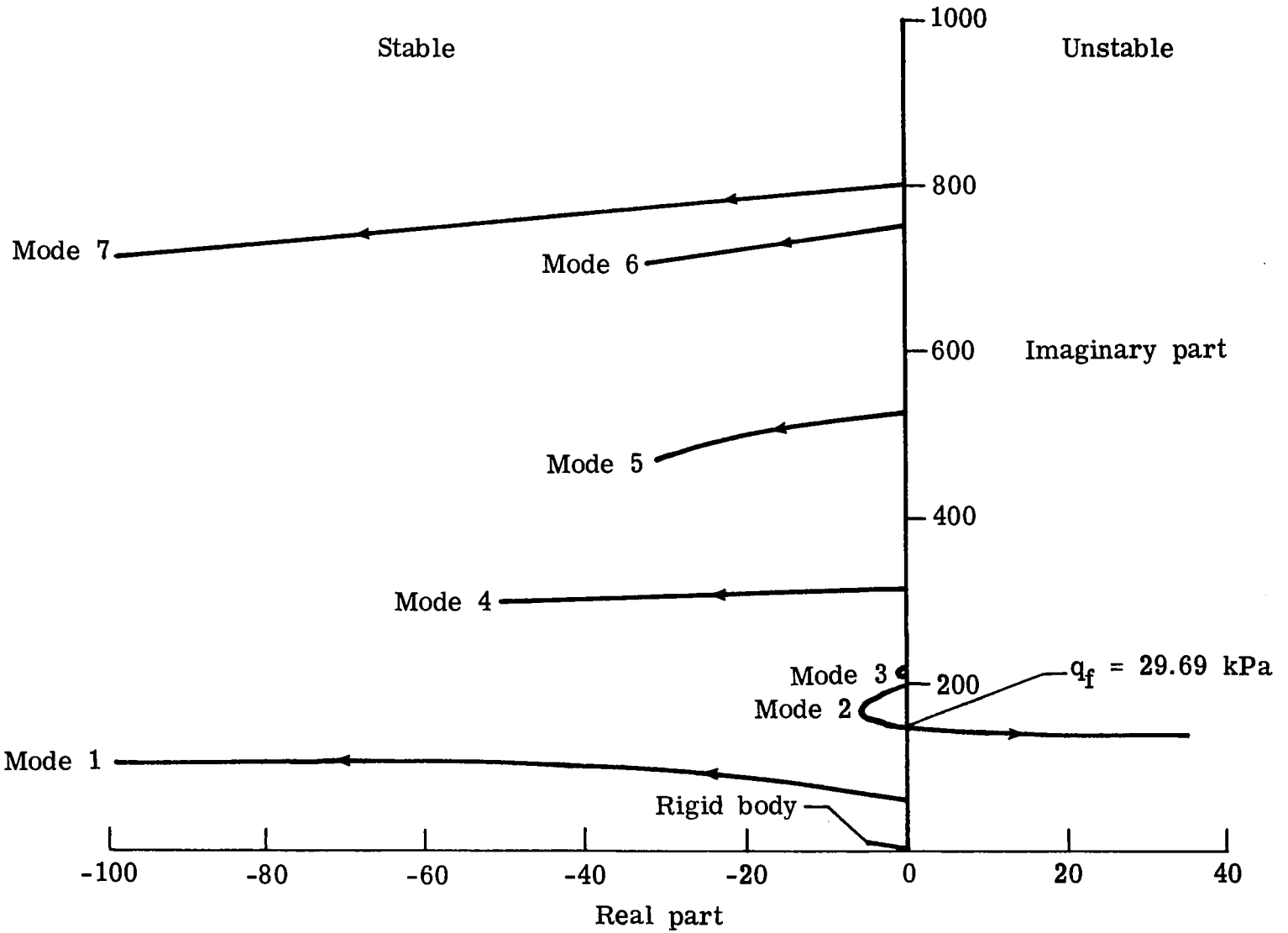

Figure 5.- Root locus plot at M = 0.5. No control. Arrows indicate increasing dynamic pressure.

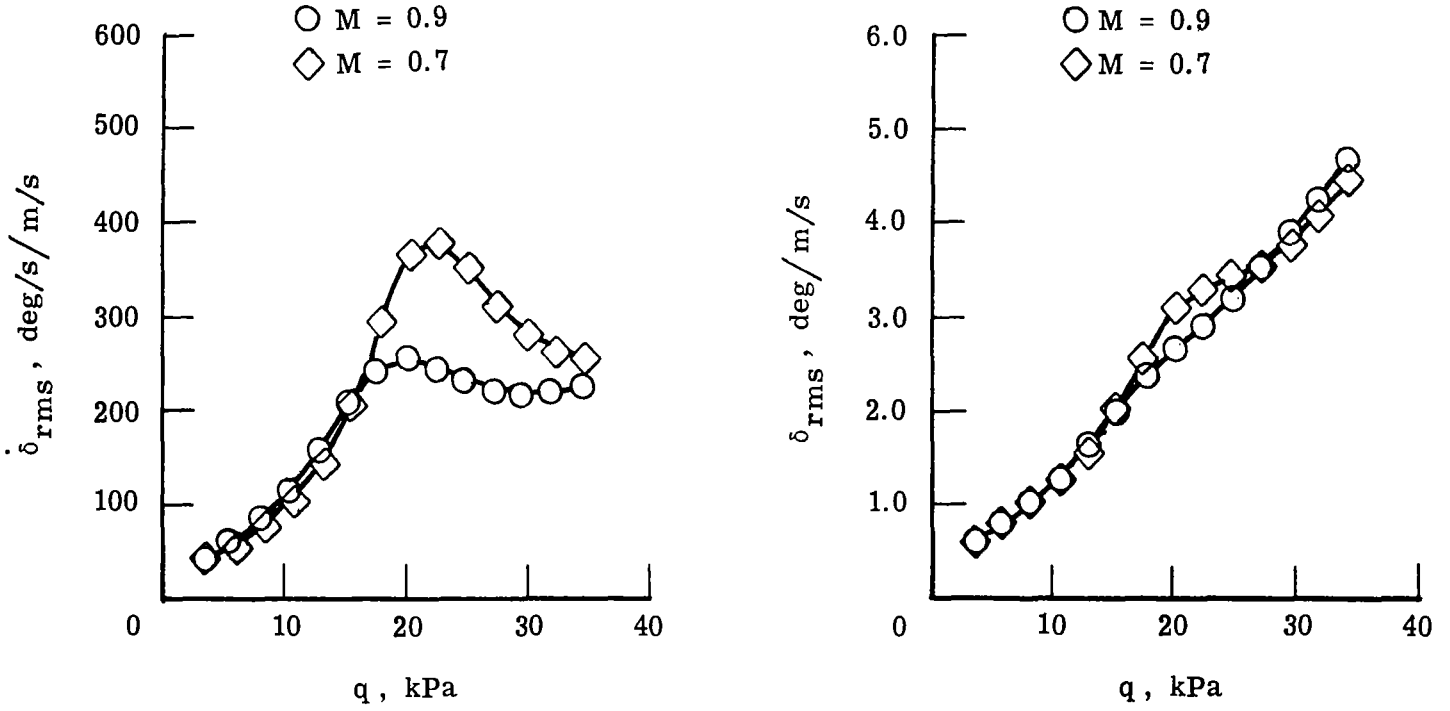

Figure 6.- Variation with q of rms response of control surface ($\omega_{n,T}$ = 25 rps) at various Mach numbers, using LDTTF.

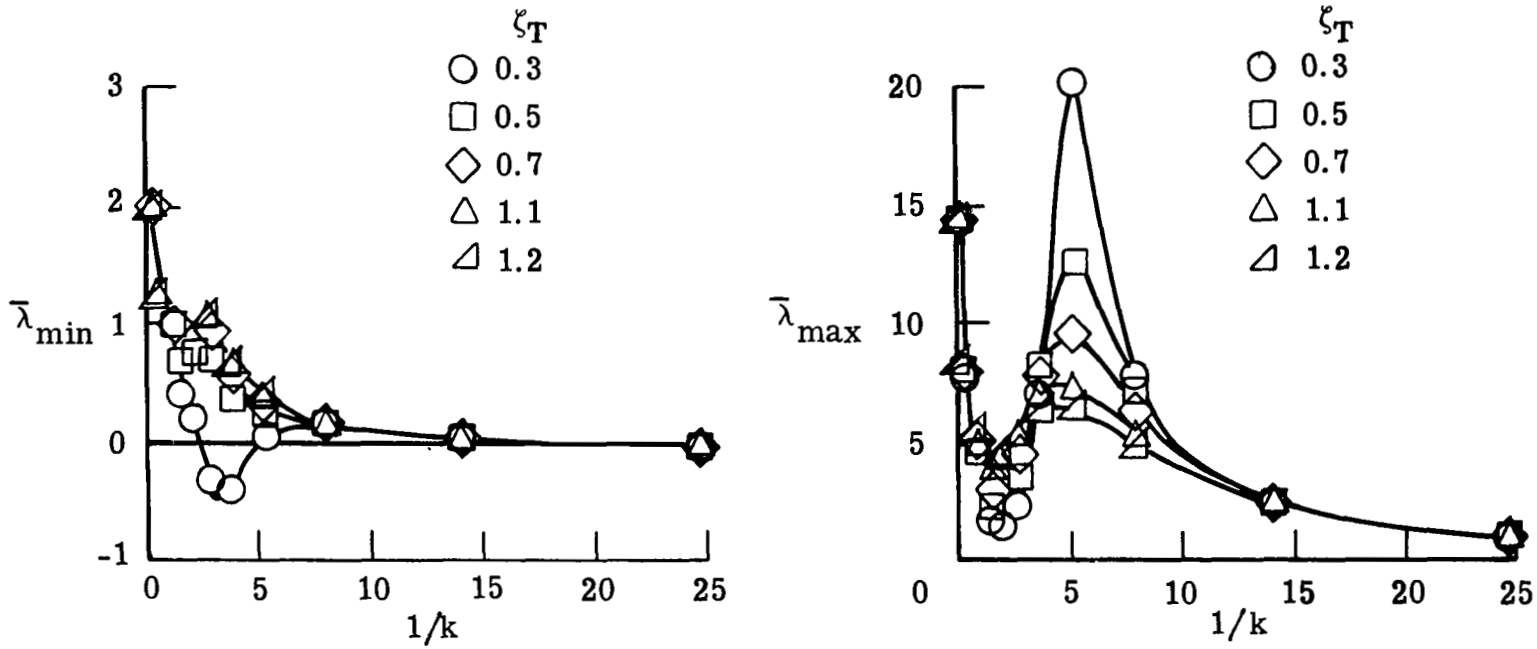

(a) $\bar{\lambda}_{min}$.

(b) $\bar{\lambda}_{max}$.

Figure 7.- $\bar{\lambda}$ as a function of 1/k for different values of ζ_T. Trailing-edge control system using LDTTF at M = 0.9 with $k_{n,T}$ = 0.2.

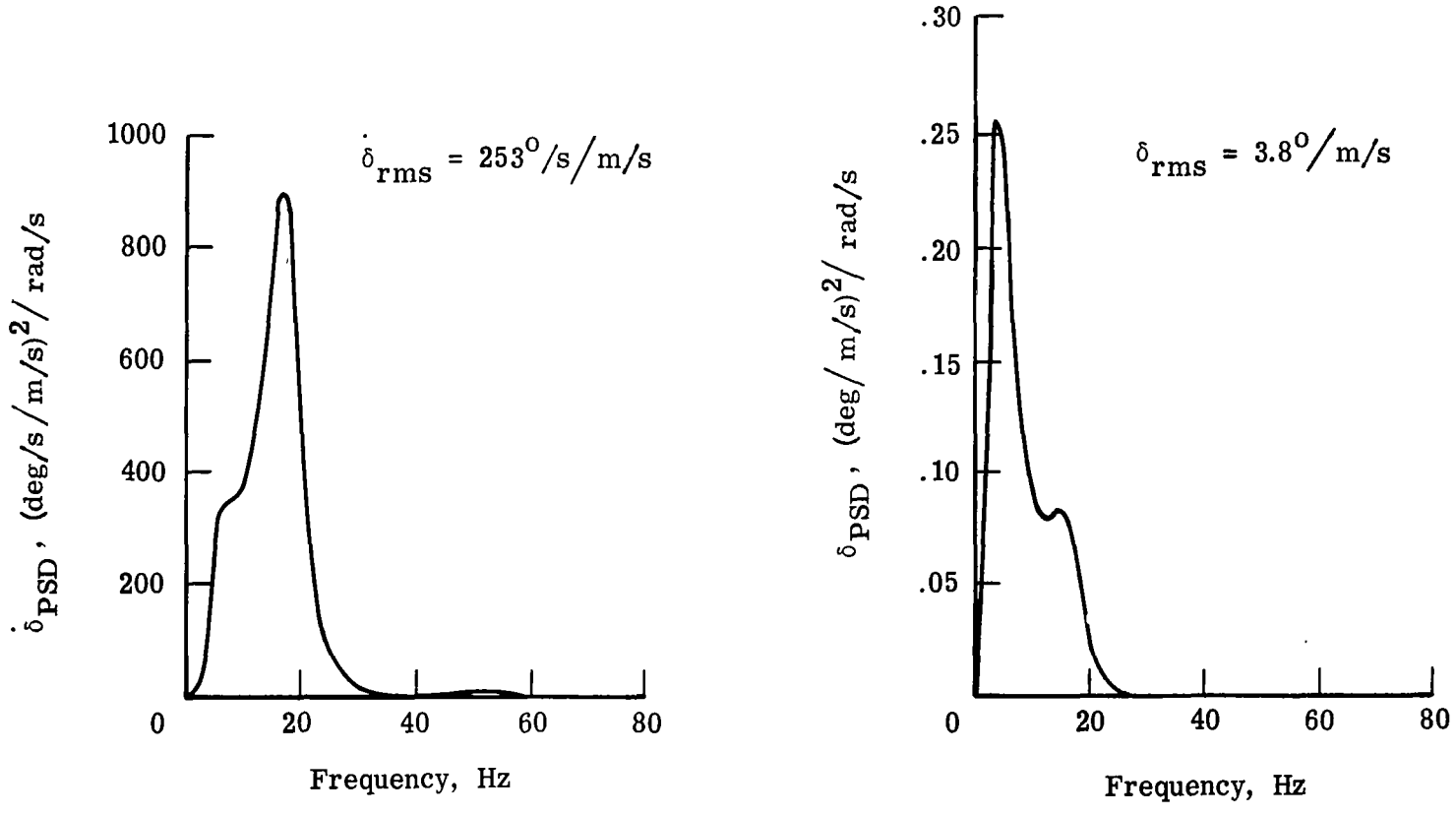

Figure 8.- Power spectral density (PSD) of control surface response at M = 0.90 using LDTTF. ($60 \leq \omega_{n,T} \leq 150$ rad/s.)

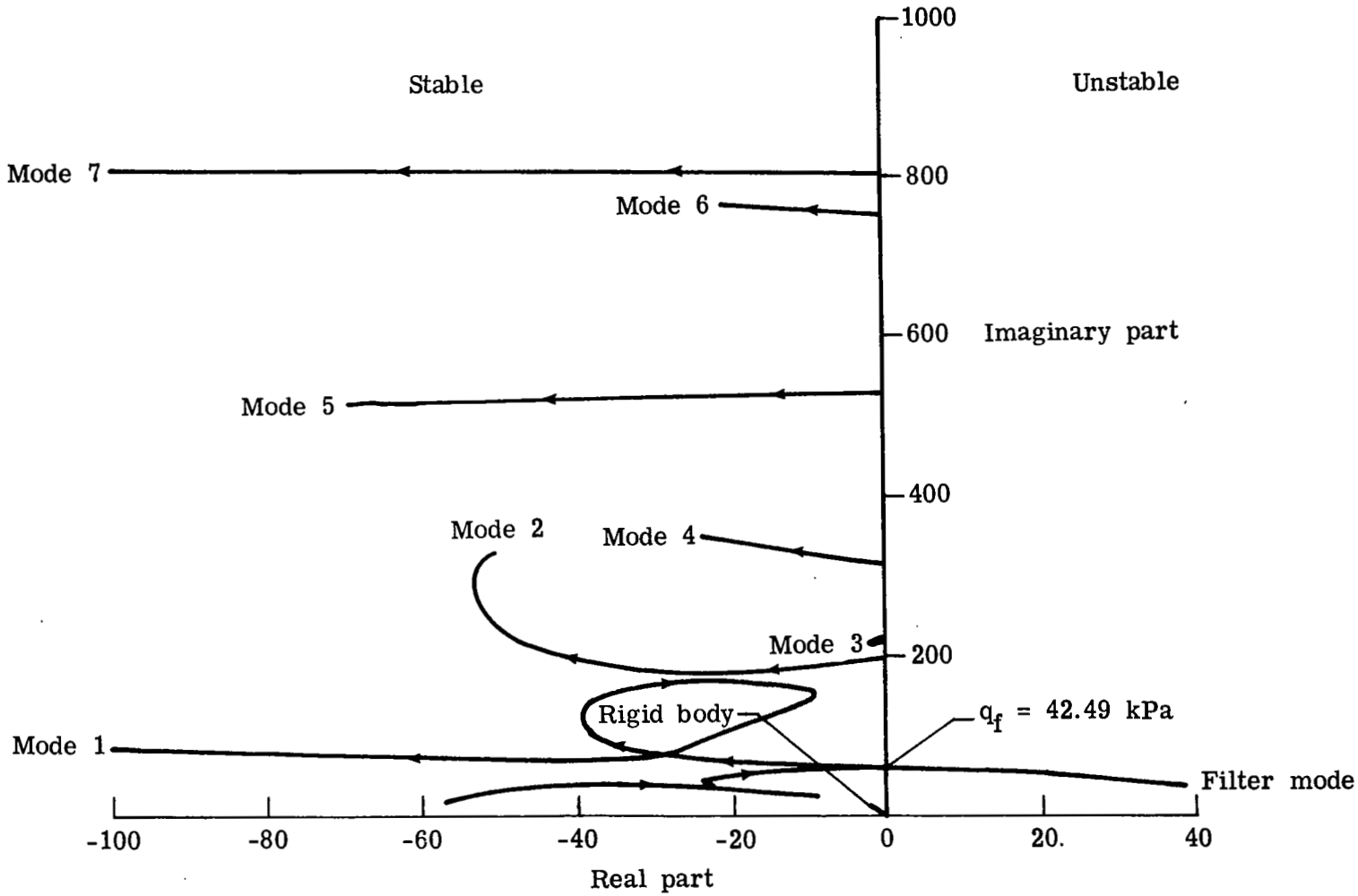

Figure 9.- Root locus plot of reoptimized trailing-edge control system at M = 0.90 using LDTTF. ($60 \leq \omega_{n,T} \leq 150$ rad/s.) Arrows indicate increasing dynamic pressure.

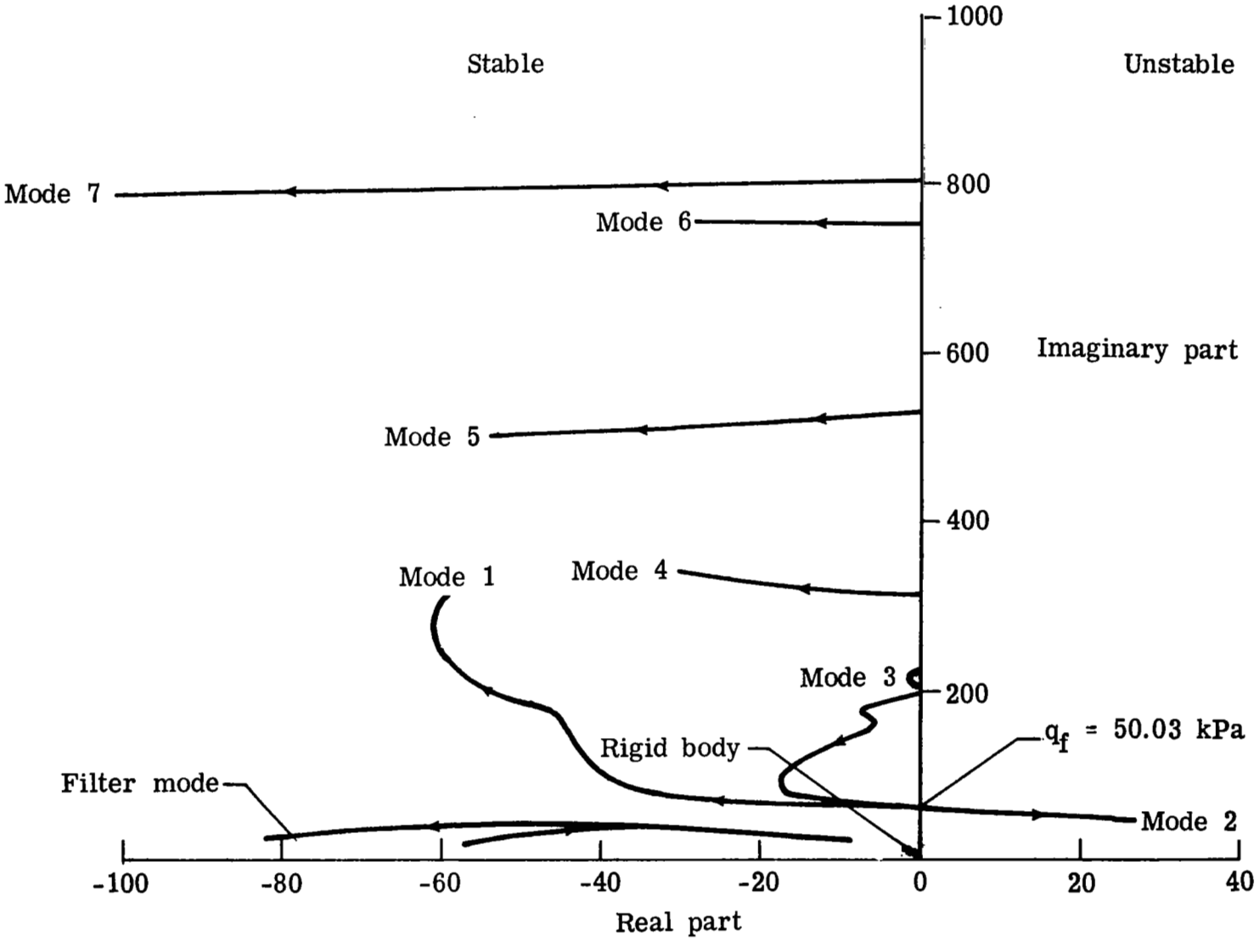

Figure 10.- Root locus plot of reoptimized trailing-edge control system at M = 0.7 using LDTTF. ($60 \leq \omega_{n,T} \leq 150$ rad/s.) Arrows indicate increasing dynamic pressure.

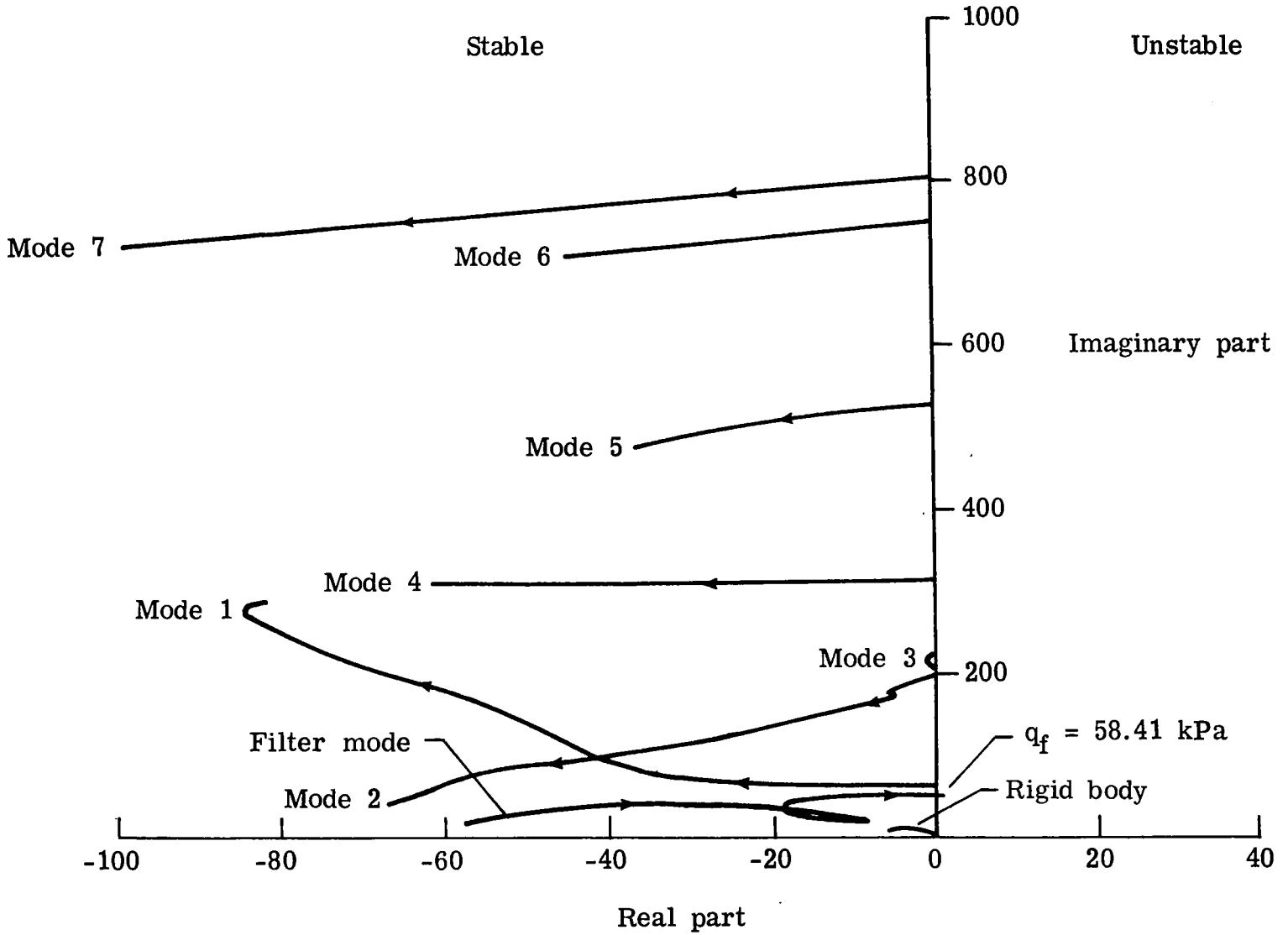

Figure 11.- Root locus plot of reoptimized trailing-edge control system at M = 0.5 using LDTTF. ($60 \leq \omega_{n,T} \leq 150$ rad/s.) Arrows indicate increasing dynamic pressure.

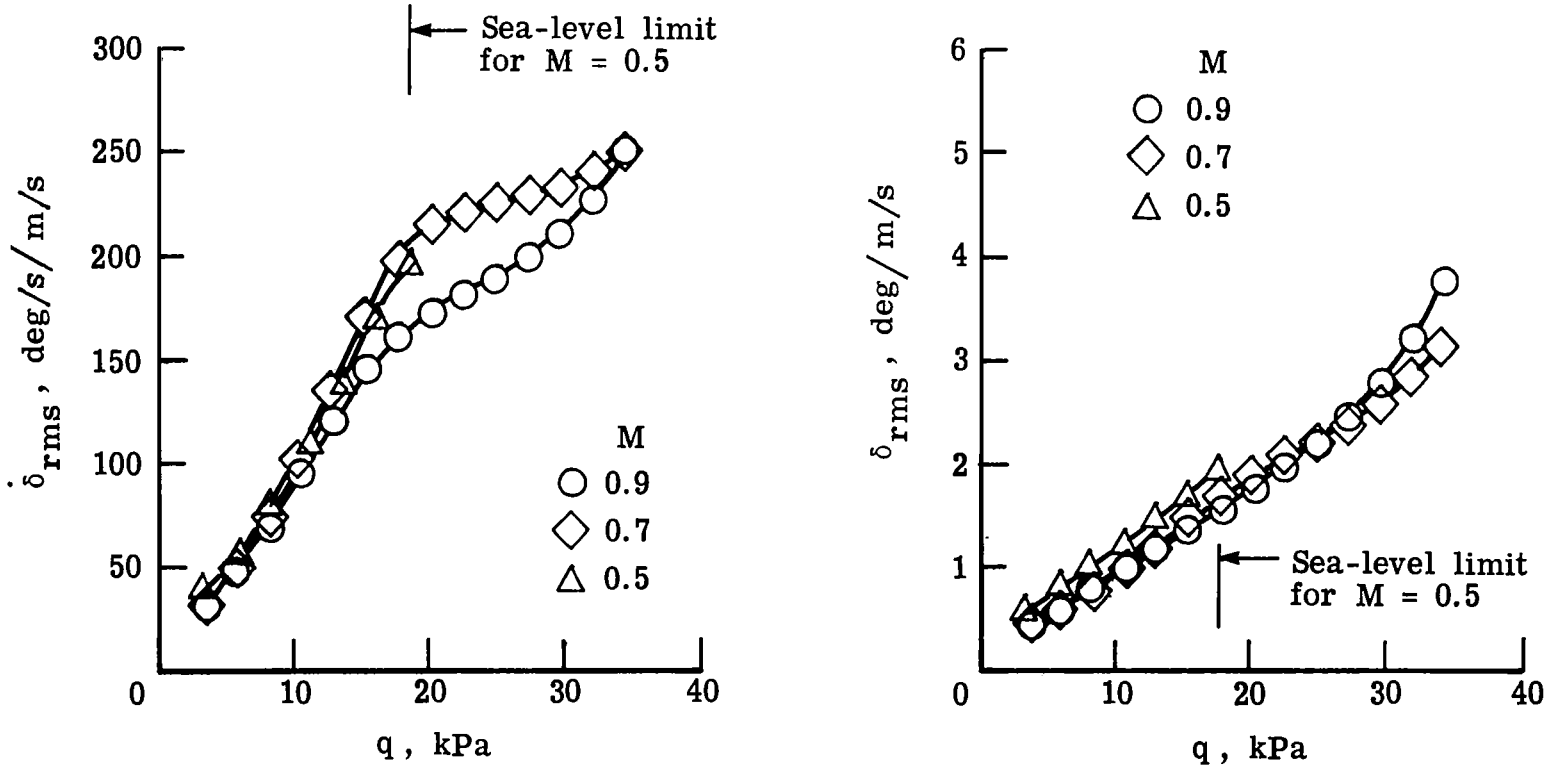

Figure 12.- Variation with q of rms response of control surface at various Mach numbers by using LDTTF. ($60 \leq \omega_{n,T} \leq 150$ rad/s.)

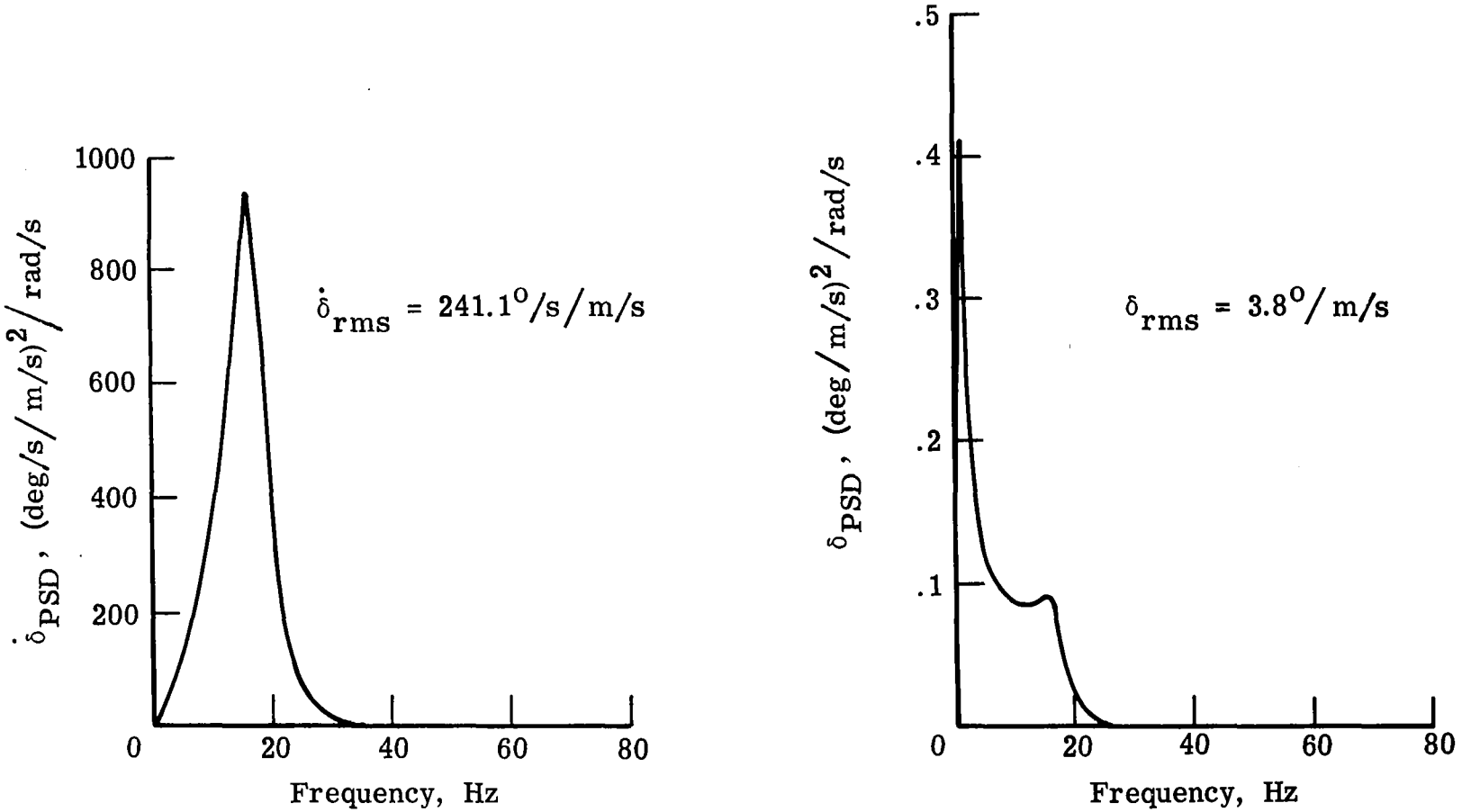

Figure 13.- Power spectral density (PSD) response of optimized control law at M = 0.90 by using DTTF.

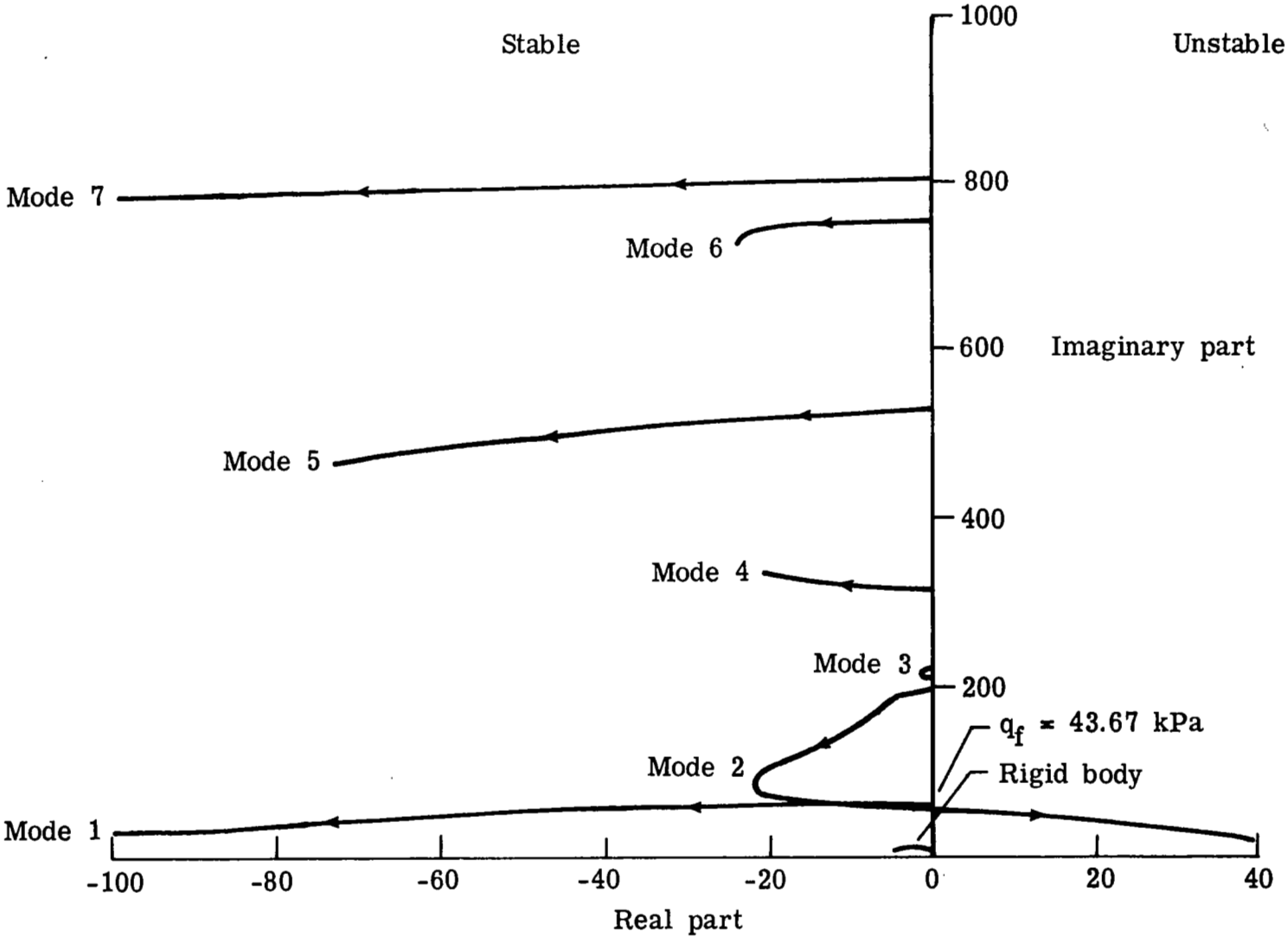

Figure 14.- Root locus plot of optimized trailing-edge control system at M = 0.9 by using DTTF. Arrows indicate increasing dynamic pressure.

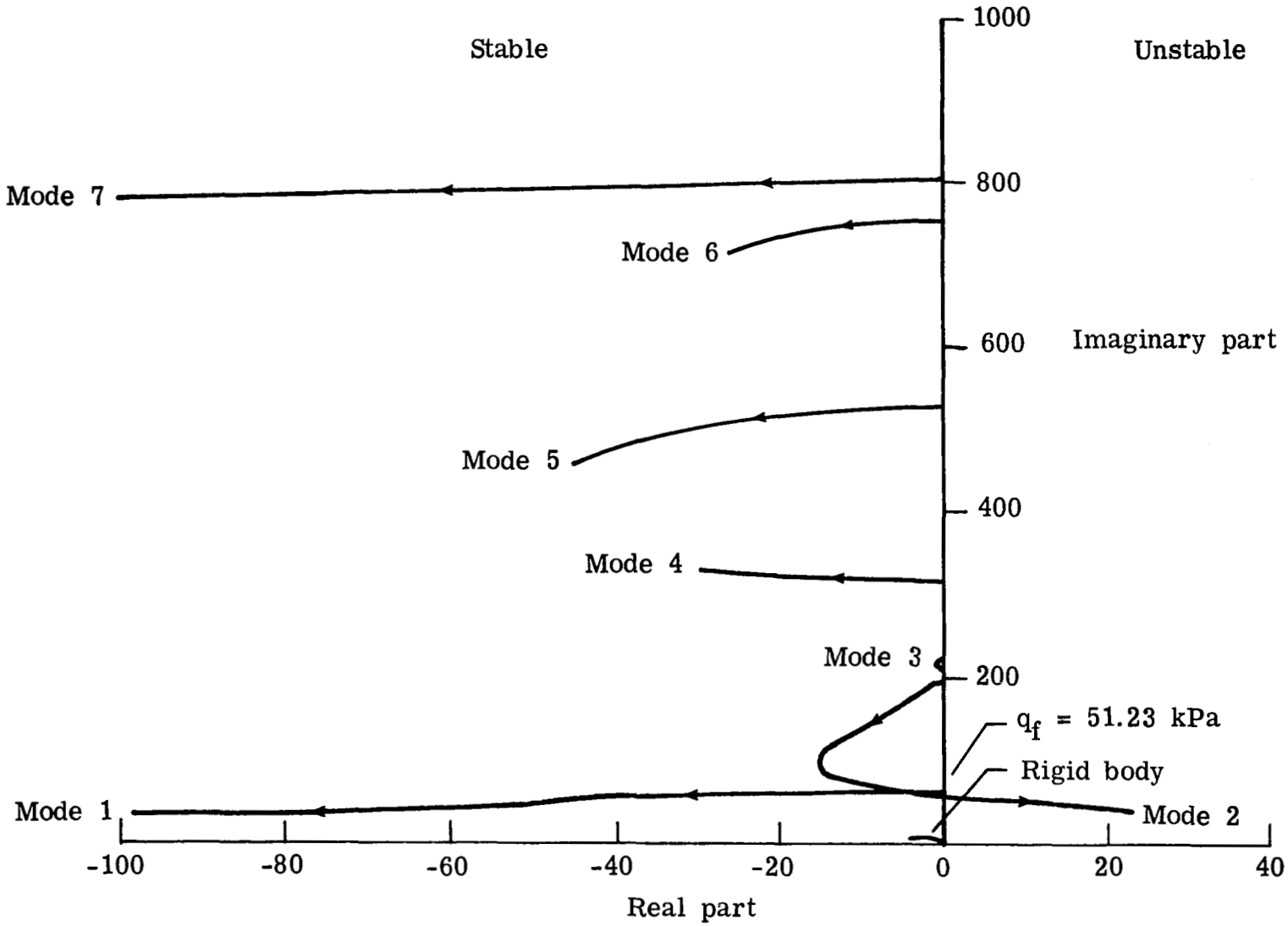

Figure 15.- Root locus plot of optimized trailing-edge control system at M = 0.7 by using DTTF. Arrows indicate increasing dynamic pressure.

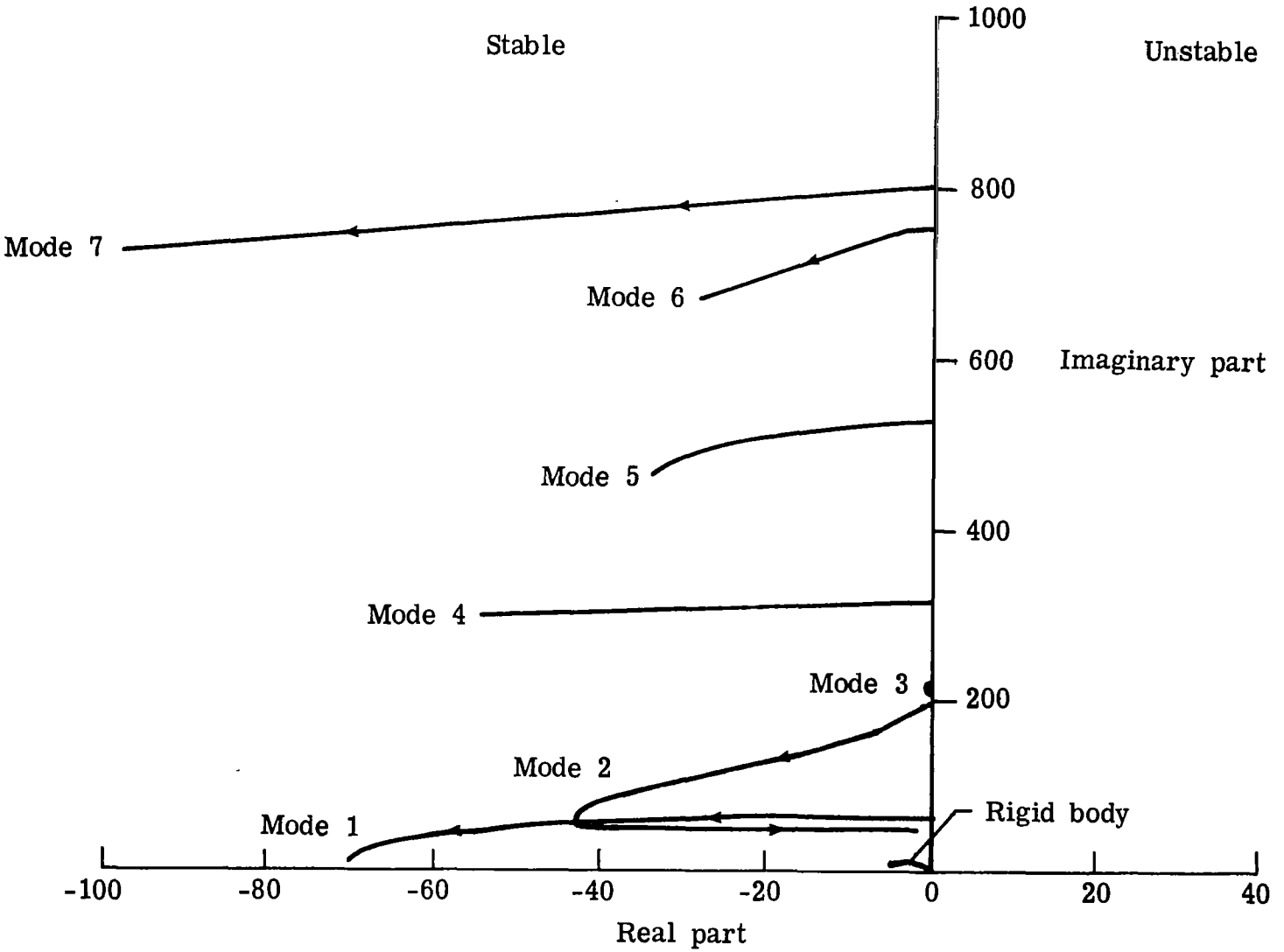

Figure 16.- Root locus plot of optimized trailing-edge control system at M = 0.5 by using DTTF. Arrows indicate increasing dynamic pressure.

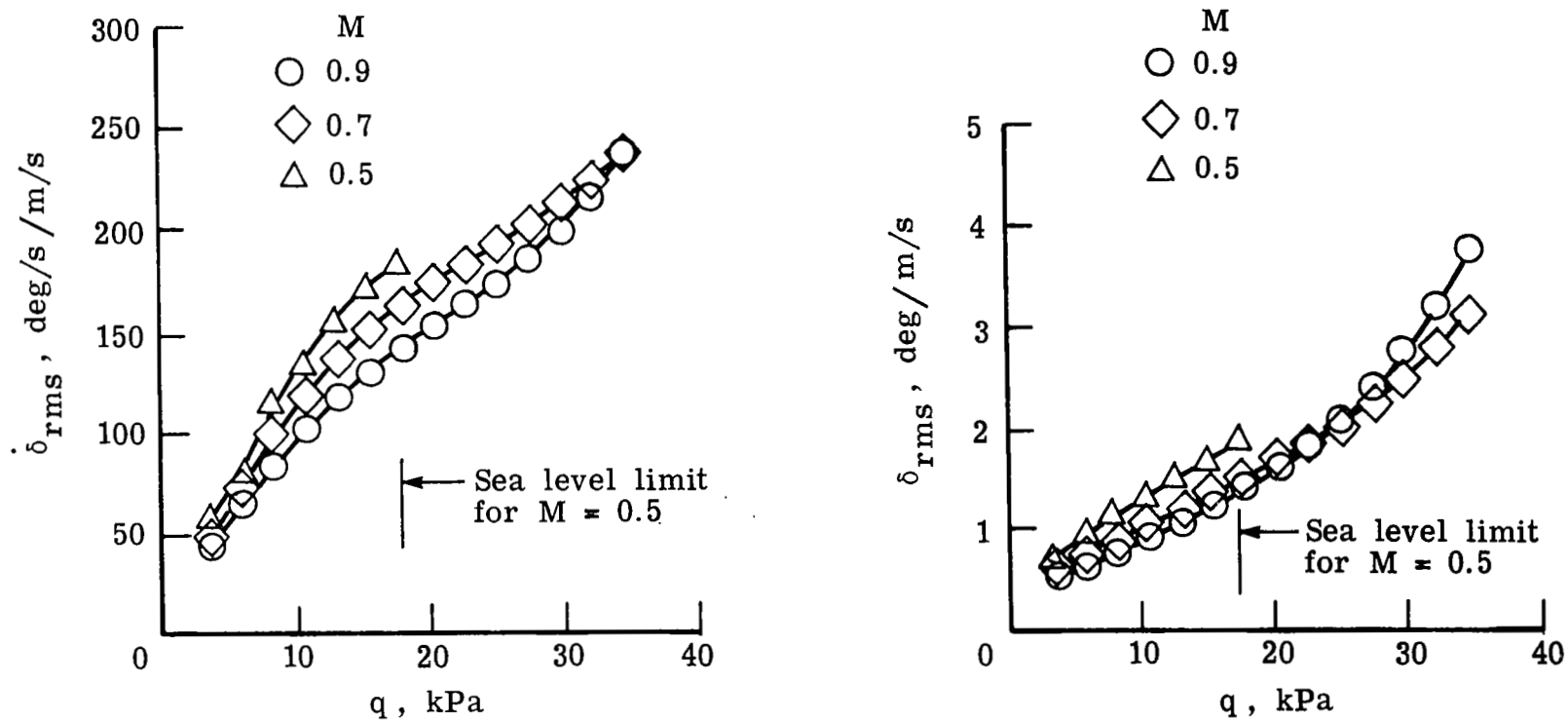

Figure 17.- Variation with q of rms response of trailing-edge control surface at various Mach numbers by using DTTF.